

Universiteit
Leiden
The Netherlands

Deciphering the complex paramagnetic NMR spectra of small laccase

Dasgupta, R.

Citation

Dasgupta, R. (2021, June 15). *Deciphering the complex paramagnetic NMR spectra of small laccase*. Retrieved from https://hdl.handle.net/1887/3188356

Version:	Publisher's Version
License:	Licence agreement concerning inclusion of doctoral thesis in the Institutional Repository of the University of Leiden
Downloaded from:	https://hdl.handle.net/1887/3188356

Note: To cite this publication please use the final published version (if applicable).

Cover Page



Universiteit Leiden

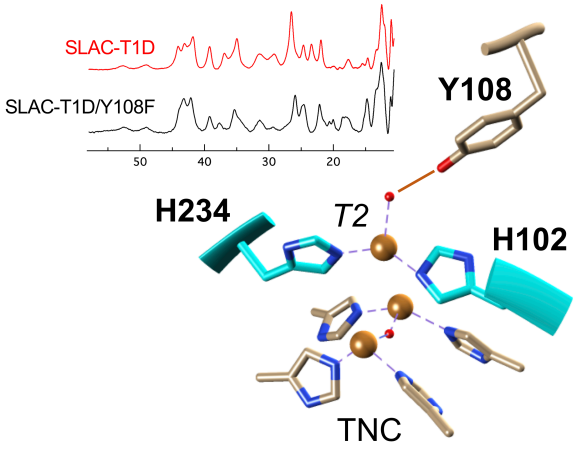


The handle https://hdl.handle.net/1887/3188356 holds various files of this Leiden University dissertation.

Author: Dasgputa, R.
Title: Deciphering the complex paramagnetic NMR spectra of small laccase
Issue Date: 2021-06-15

Chapter 3

Towards resolving the complex paramagnetic NMR spectrum of small laccase: Assignments of resonances to residue specific nuclei



This chapter is published as:
Dasgupta, R., K.B.S.S. Gupta, H.J.M. de Groot, and M. Ubbink. 2021. Towards resolving the complex paramagnetic nuclear magnetic resonance (NMR) spectrum of small laccase: assignments of resonances to residue-specific nuclei. *Magnetic Resonance*. 2:15–23. DOI: https://doi.org/10.5194/mr-2-15-2021

Laccases efficiently reduce dioxygen to water in an active site containing a tri-nuclear copper centre (TNC). The dynamics of the protein matrix is a determining factor for the efficiency in catalysis. To probe mobility, NMR spectroscopy is highly suitable. However, several factors complicate the assignment of resonances to active site nuclei in laccases. The paramagnetic nature causes large shifts and line broadening. Furthermore, the presence of slow chemical exchange processes of the imidazole rings of copper ligands results in peak doubling. A third complicating factor is that the enzyme occurs in two states, the native intermediate (NI) and resting oxidized (RO) states, with different paramagnetic properties. The present study aims at resolving the complex paramagnetic NMR spectra of the TNC of *S. coelicolor* small laccase (SLAC). With a combination of paramagnetically tailored NMR experiments, resonances of all eight His Nδ1 and Hδ1 for the NI state are identified, as well as His Hβ protons for the RO state. With the help of second shell mutagenesis, selective resonances are tentatively assigned to the histidine ligands of the copper in the type-2 site. This study demonstrates the utility of the approaches used for the sequence specific assignment of the paramagnetic NMR spectra of ligands in the TNC that ultimately may lead to a description of the underlying motion.

3.1 Introduction

Multicopper oxidases (MCOs) oxidize a wide variety of substrates at their type 1 (T1) site and catalyse the 4-electron reduction of molecular oxygen to water at the tri-nuclear copper center (TNC). The TNC consists of a type 2 (T2) copper site and a binuclear type 3 (T3) copper site. Based on crystallographic, spectroscopic and theoretical studies, the present model of the oxygen reduction mechanism by the TNC is shown in Figure 1.3.(1–5) The two-domain small laccase from *S. coelicolor* (SLAC) has been reported to involve the formation of a tyrosine radical (Tyr108$^{\bullet}$) near the T2 site during the peroxide intermediate (PI) to native intermediate (NI) conversion.(1, 4) This radical has been suggested to act as protection against the reactive oxygen species (ROS) that can be formed due to the long-lived peroxide intermediate state.(1, 6) The tyrosyl radical was shown to be reduced by the protein environment via tryptophan and tyrosine residues around the T2 site.(6) A similar role was proposed for Tyr107 in human ceruloplasmin (hCp). hCp is a ferroxidase critical for iron homeostasis. It oxidizes Fe^{2+} to Fe^{3+} for iron transport. In serum the hCp is active under low Fe^{2+} and high O_2 concentration. This leads to a partially reduced intermediate that can form ROS. The tyrosine radical protects the protein from this partially reduced state.(7)

Although the reaction mechanism of laccase is well characterized, information about motions around the TNC is limited. The oxygen reduction process

is a multi-step reaction involving transfer of four electron and protons with oxidation and reduction of the copper ions (Figure 1.3). Each step is associated with its respective activation energy barrier and the motions of the protein, especially within the active site, may be useful in reduction or crossing of these barriers. Such motions have been reported for many proteins, for example dihydrofolate reductase, adenylate kinase and cytochrome P450.(8–11) Characterisation of the motion at the TNC of laccase can help in designing a functional framework for understanding the natural process and the *de novo* design of efficient bioinspired catalysts. Three or more independent chemical exchange processes, tentatively assigned to the coordinating histidine residues at the TNC were reported using paramagnetic NMR spectroscopy on the T1 copper depleted variant of SLAC, SLAC-T1D (Chapter 2).(12) However, further characterisation of motions requires assignments of the NMR resonances very near to the TNC. The paramagnetic nature of the copper ions causes broadening and chemical shifts outside of the diamagnetic envelope, making it impossible to employ standard multidimensional protein assignment experiments. Assignment is further complicated by two reasons. SLAC spectra are a mixture of the RO and NI states. (13) In the RO state the T2 Cu^{2+} is isolated, causing broadening of the signals of nearby proton spins beyond detection. The two copper ions in the T3 site are antiferromagnetically coupled, with a low-lying triplet state that is populated at room temperature, causing paramagnetically shifted (in the range of 12 - 22 ppm), detectable resonances of nearby protons. In the NI state all copper ions are coupled, resulting in a frustrated spin system, with strongly shifted (> 22 ppm), but observable resonances.(14) The second cause of complexity is that the mentioned exchange processes of the coordinating histidine residues result in peak doublings, because the exchange rates are in the slow exchange regime relative to the resonance frequency differences. In this study, we aimed to resolve further this complicated paramagnetic NMR spectrum. Using differently labelled samples and tailored HMQC experiments, the presence of all eight-histidine ligand Nδ1 and Hδ1 resonance in the NI state could be established. The first studies of the RO state identified resonances as histidine Hδ1 or Hβ protons and a second coordination shell mutant allowed for the first residue and sequence specific assignment. The study demonstrates the utility of the approaches used for the sequence specific assignments of the ligands in the TNC that may ultimately lead to a description of the underlying motions.

3.2 Results and discussions

Identification of nitrogen attached protons in the NI state

The Fermi contact shifted resonances for SLAC-T1D were reported before and here we use the numbering used in our previous study (Chapter 2).(12, 13) Eighteen resonances were found between 15 and 60 ppm.(12) Resonances 1 and 2 were assigned to a region that is attributed to the RO state, therefore we followed the numbering from 3 to 18 in the present work (Figure 3.1a and 2.1a). Resonance 10 is from a proton bound to carbon and is overlapping with resonances 9 and 11 at temperatures > 293 K (12) (Figure 3.1a). The ^{1}H resonances that exhibited exchange processes (3-5, 9-11 and 13-12, see also Figure 2.2 and S2.2) were assigned to Hδ1 nuclei from histidine coordinated to the copper ion (Chapter 2). To verify this assignment, a paramagnetically tailored ^{15}N – ^{1}H HMQC experiment (Figure 1.5c, the detail of the experiment is given in the caption of Figure S3.2) was performed on a SLAC-T1D sample that was specifically labelled with ^{15}N histidine in a perdeuterated, back-exchanged environment. The evolution period was shortened to 500 μs, balancing the time required for formation of antiphase magnetisation and paramagnetic relaxation, to optimize S/N ratio for most of the resonances.(15, 16) A total of 10 resonances (3, 4, 5, 6, 9, 11, 12, 13, 14/15, 16, see Figure 3.1b) were observed at ^{1}H chemical shifts of > 21 ppm. Resonance 7, 8 and 10 were not observed in this experiment, which is consistent with their assignment to carbon attached protons (Chapter 2).(17) These results show unequivocally that the HMQC resonances derive from the Hδ1 protons of the coordinating histidine residues of the TNC, because only these protons are nitrogen attached and close enough to experience such large paramagnetic shifts. The three pairs or resonances representing exchange processes (3-5, 9-11 and 13-12) are thus also from Hδ1 proton, in line with the suggested histidine ring motion being the involved chemical exchange process. The HMQC spectrum of uniformly ^{15}N labelled SLAC-T1D is similar to the ^{15}N-His specifically labelled SLAC-T1D sample in a perdeuterated back-exchanged environment (data not shown for the ^{1}H resonances > 21 ppm but shown for the region 12 to 21 ppm, see Figure 3.2b).

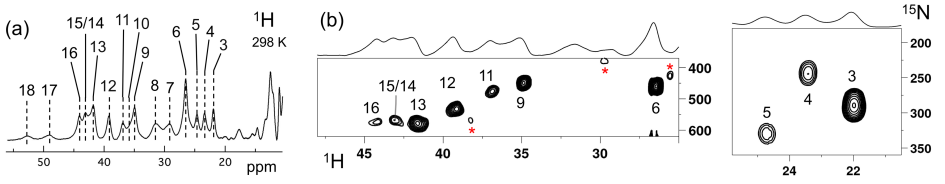


***Figure 3.1**. SLAC-T1D NMR spectra at 298 K. (a) 1D ^{1}H WEFT spectrum of SLAC-T1D and (b) ^{15}N-^{1}H HMQC spectra of ^{15}N-His perdeuterated SLAC-T1D in a back-exchanged environment. The numbering is adopted from (17). Noise peaks in the spectrum are marked with a red asterisk. The 1D ^{1}H WEFT spectrum is shown above the HMQC spectrum.*

The relative intensities of signals in the range 60-22 ppm with those of the region 21-12 ppm shows that SLAC-T1D is predominantly in the NI state (Figure 3.1 and 3.2). In the NI state, the T2 and the T3 sites are coupled thereby increasing the electronic relaxation rates of the unpaired electron spin S of the T2 site. This results in the reduction of the paramagnetic relaxation rates of the neighbouring nuclear spins. (18, 19) Therefore, it is expected that all eight ligand histidine residues are observable. In the ^{15}N–^{1}H HMQC ten resonances are seen, among which three undergo chemical exchange resulting in the observation of seven Nδ1-Hδ1 group. Resonance 17 and 18 have exchange cross-peaks with resonance 15/14 and 16, respectively at high temperatures (303 K and 308 K) and a short mixing time in an EXSY/NOESY experiment (1 and 2 ms) (Chapter 2, Figure S2.4).(17) At temperatures of 298 K and higher, resonances 14 and 15 overlap (Figure 3.1a).(17) Resonance 16 and 18 thus form a fourth exchange pair and the seventh histidine Nδ1-Hδ1 group. The eighth histidine Nδ1-Hδ1 group can be attributed to the exchange pair of resonance 17 with either 14 or 15.(17) Due to the overlapping of resonance 14 and 15 at 298 K, they are not observed distinctly in ^{15}N–^{1}H HMQC spectra (Figure 3.1b). In conclusion, all the eight Hδ1 from the coordinating histidine ligands of the TNC in SLAC-T1D for the NI state are identified in the spectral region > 21 ppm and five of them show peak doubling due to slow exchange.

Analysis of the RO state

Machczynski *et al*. (2016) reported that the signals in the spectral region between 12 to 21 ppm derive from the RO state, whereas the resonances > 21 ppm are attributed to the NI state.(13) In the RO state, the T2 copper is decoupled from the T3 site, resulting in a decrease of its electronic relaxation rate.(18) This effect broadens the resonances of nearby proton spins beyond detection for the T2 site ligands. In the RO state, the T3 copper ions are antiferromagnetically coupled and thus diamagnetic at low temperature.(18) At ambient temperature, the low-lying state with $S = 1$ is populated, resulting in paramagnetic shifts of the ligand protons.(18) The strong coupling via a hydroxyl group of the electron spins causes fast electronic relaxation and thus observable nuclear resonances for T3 ligands. T3 site ligands usually exhibit an anti-Curie behaviour, i.e. the chemical shift increases with an increase in temperature.(19–21)

All the resonances in the 12 to 22 ppm region of SLAC-T1D in an ^{1}H-^{1}H EXSY/NOESY spectrum display anti-Curie behaviour, suggesting that indeed they

derive from histidine protons of the T3 site (Figure 3.2). Comparing the ^{15}N–^{1}H HMQC and the ^{1}H-^{1}H EXSY/NOESY of the ^{15}N uniformly labelled sample in this region, resonances a1, a2, b2, c1, c2, d2, x1, x2, y, z and w are nitrogen linked protons (Figure 3.2). The RO state is the minor state in SLAC-T1D, so the S/N ratio for the HMQC resonances is low. For comparison, resonance 3, which belongs to the NI region of the spectrum (Figure 3.2b) is shown as well. ^{1}H resonances e1 and e2 could not be assigned to either carbon or nitrogen linked protons due to their low S/N ratio.

Using a two-metal center model to calculate the singlet-triplet energy gap ($2J$) from the temperature dependence of the chemical shifts (equation 1.5), a $2J$ value of -600 +/- 20 cm^{-1} was obtained, within the range of the previous reported values (-550 to -620 cm^{-1}) for the RO state of laccase (Figure 3.2c) (3, 13, 22). It was assumed that resonances a1, a2, b2, c1, c2, d2 (only isolated resonances were selected) are the Fermi contact shifted resonances of the Hδ1 of the coordinating histidine residues at the T3 site in the RO state (Figure 3.2d), as supported by their presence in the HMQC spectrum (Figure 3.2b). The diamagnetic chemical shift for these resonances was set to 9.5 ppm (BMRB average for histidine ring Hδ1).(14) To establish the diamagnetic chemical shifts of resonances b1 and d1, which are not nitrogen attached, the $2J$ coupling strength was then fixed to -600 cm^{-1} and the diamagnetic chemical shift was fitted and found to be 3.0 +/- 0.5 ppm. This value strongly suggests that these resonances are from the eight protons of coordinating histidine ligands (BMRB average for histidine Hβ is 3.1 ppm).

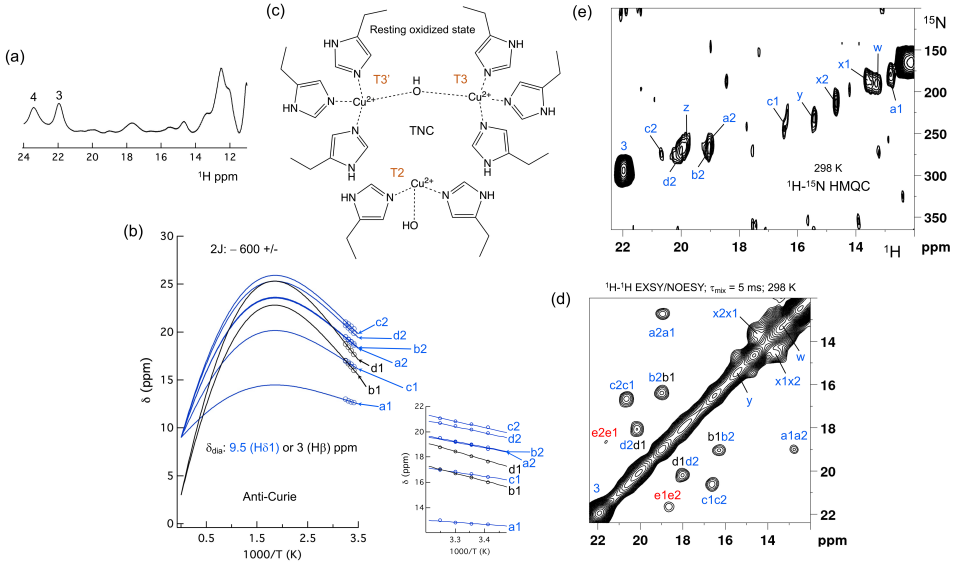


***Figure 3.2**. The spectral region of the RO state. (a) 1D ^{1}H spectra of the RO region from panel a of Figure 1. Resonances 3 and 4 of the NI spectral region are shown for comparison; (b) Temperature dependence of the chemical shift for the resonances a1, a2, b1, b2, c1, c2, d1 and d2, fitted to the two-metal center model (equation 1.5). The inset shows the experimental region of the fit. The corresponding hyperfine coupling constants are given in Table S3.5 of the supporting information; (c) Schematic representation of the RO state of the TNC. The T3 and T2 copper ions are marked. (d) ^{1}H-^{1}H EXSY/NOESY spectra of SLAC-T1D for the region between 12 to 22 ppm; (e) ^{15}N-^{1}H HMQC spectra of the ^{15}N uniformly labelled SLAC-T1D (12 to 22 ppm in the ^{1}H dimension). The resonances marked in blue are for the nitrogen attached protons while resonances in black are for carbon attached protons. Resonances in red in panel d could not be assigned to either nitrogen linked or carbon linked protons due to a low S/N ratio.*

Since the temperature dependence of the cross peak intensities as measured by their peak volume did not show a conclusive increasing trend with increase of temperature, we assumed them to be NOE rather than EXSY derived cross-peaks.(17) Therefore, the cross peaks of resonances b1-b2 and d1-d2 can be attributed to a NOE between the Hδ1 and Hβ proton of a histidine ligand. The cross-peaks between c1-c2 and a1-a2 appear to be NOE signals from nitrogen attached protons (Figure 3.2). The Hδ1 protons of the different histidine residues are not near, so it remains unclear from which spins these peaks derive. For the resonances x1, x2, y, z and w (Figure 3.2a) the analysis of the temperature dependence of the chemical shift was not possible due to the overlap.

Second shell mutagenesis to assist assignments

To aid in the assignment of the paramagnetic spectrum, mutagenesis could be employed. However, mutation of histidine ligands is expected to result in loss of copper or at least in a severe redistribution of unpaired electron density, changing the chemical shifts of all paramagnetically shifted protons. In contrast, mutations in the second coordination sphere, of residues that interact with the coordinating ligands, may have moderate effects on the electron spin density distribution. One such mutant, Y108F, has been reported before.(1) Tyr108 interacts with the TNC in two ways, with the T2 site through the water/hydroxide ligand and with the T3 ligand His104 through the hydrogen bonding network involving Asp259 (Figure S3.3a). Asp259 is conserved in all laccases, whereas Tyr108 is conserved in the two-domain laccases (Figure S3.3b). Asp259 has been reported to play a role in modulating the proton relay during the oxygen reduction reaction (23) and it may also stabilize the Tyr108-TNC interaction.

The 1D ^{1}H WEFT (24, 25) spectrum of SLAC-T1D/Y108F is similar to that of SLAC-T1D, suggesting that the variant SLAC is also predominantly in the NI state (Figure 3.2a). Some changes in the chemical shift are present. Due to the Y108F

mutation many of the ^{1}H resonances > 22 ppm are downfield shifted. Resonance 6 and 16 are upfield shifted and resonance 7, 8, 17 and 18 show no chemical shift change compared to SLAC-T1D (Figure 3.3 and Table S3.2). Also, a new resonance α is observed. The HMQC spectrum in the region > 22 ppm of the ^{1}H is very similar to that of SLAC-T1D, in agreement with the ^{1}H WEFT spectrum (Figure 3.3). Most of the ^{15}N resonances (3, 4, 5, 9, 11, 12 and 15) are downfield shifted except resonances 6, 13 and 16, which are upfield shifted (Figure 3.3 and Table S3.2). The three independent chemical exchange processes that were reported for the TNC of SLAC-T1D involving resonance pairs of 3 – 5, 9 – 11 and 13 – 12 (Chapter 2, Figure 2.2) are conserved and the rates are not affected by the Y108F mutation (Table S3.1, Figure 3.3b and Figure S3.1c), suggesting that the phenolic –OH group of Y108 is not involved in the chemical exchange process.(17) The chemical shift changes show that the two states represented by 3 – 5 and 9 – 11, respectively are affected similarly by the Y108F mutation (Figure 3.3d). In contrast, the two states represented by the resonance pair 13 – 12 are affected differently, because the nitrogen chemical shift is downfield shifted for resonance 12 and to upfield shifted for resonance 13 (Figure 3.3d).

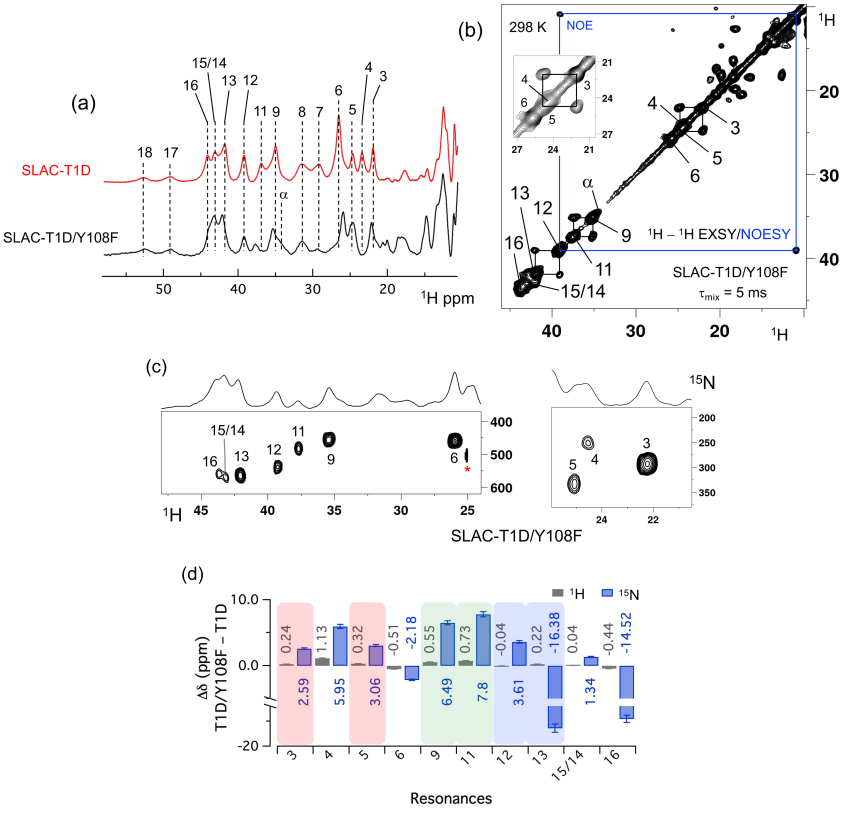


***Figure 3.3**. Spectra of SLAC-T1D/Y108F. (a) Comparison between 1D ^{1}H WEFT spectrum of SLAC-T1D (red) and SLAC-T1D/Y108F (black). The numbering is shown for SLAC-T1D and is adopted from (17); (b) ^{1}H-^{1}H EXSY/NOESY of SLAC-T1D/Y108F at 298 K with mixing time of 5 ms. NOE cross-peaks are connected with a blue rectangle. The remaining cross-peaks are exchange peaks. This distinction is based on the temperature dependent profile of the integral volume of the cross peaks as explained in (17). The inset shows that the exchange cross peaks are between 3 and 5. Resonance 4 is partly overlapping with 5; (c) ^{15}N-^{1}H HMQC spectra of ^{15}N uniformly labelled SLAC-T1D/Y108F; (d) The chemical shift changes ($\Delta\delta$) between SLAC-T1D/Y108F and SLAC-T1D for the ^{1}H (black) and ^{15}N (blue). The error bars represent the standard deviation in the determination of the chemical shift. The three pairs of resonances displaying chemical exchange are highlighted by equal background colours. Positive (negative) values represent shift to the downfield (upfield) ppm for SLAC-T1D/Y108F.*

It is proposed that resonances 13 and 16, which are most affected by the Y108F mutation (Figure 3.3d), are from the histidine ligands of the T2 copper. Due to the proximity of the T2 copper and strong hydrogen bond with a water or hydroxide ligand, the electron spin density can be expected to be delocalized to the tyrosine ring. The loss of the hydrogen bond between the phenolic -OH group of Tyr108 and the water/hydroxide ligand of the T2 copper can result in redistribution of the electron spin density on the coordinating histidine ligands. Figure 3.3d shows that the Nδ1 of the resonances 13 and 16 have the highest chemical shift perturbation of ~ –16 and –14 ppm respectively. Interestingly, resonance 13 is in an exchange process with resonance 12 (Figure 3.3b) (17) and for the latter resonance the Nδ1 exhibits a downfield shift due to the Y108F mutation. In the crystal structure 3cg8 (resolution 2.63 Å), the Nδ1 of His102 from the T2 site can have two hydrogen bonding partners, carbonyl oxygen of Asp113 and a water molecule (Figure 3.4a). Modelling the protons and changing the $\chi 2$ dihedral angle of His102 to –152° and –94°, hydrogen bonds can be formed between Hδ1 — Asp113 CO and Hδ1 — H_2O respectively. The $\chi 2$ dihedral change does not break the coordination of His102 Nε2 to the copper (Figure 3.4b and 3.4c) and is within the allowed range (–90° to –170°) (17). This shows that there can be a conformational exchange of His102 between two states with a hydrogen bond between Hδ1 and either Asp113 CO or the nearby H_2O molecule. The second shell mutation of Y108F suggests that the exchanging resonances 13 and 12 are from a Hδ1 nucleus of one of the two T2 copper histidine ligands. Thus, it is proposed that resonance 13 and 12 are from His102 Hδ1 for which the ring exchanges between the two states shown in panels Figure 3.4b and 3.4c. Consequently, resonance 16 can be tentatively assigned to the other T2 copper ligand, His234, being also strongly affected by the Y108F mutation. It does not exhibit chemical exchange at temperatures ≤ 298 K, in agreement with having a single, hydrogen bond with Asp259 CO (Figure 3.4a).

At higher temperatures (≥ 303 K) however, exchange with resonance 18 is observed. Whereas the 12/13 pair of resonances shows a difference of less than 3 ppm (17) and similar linewidth for both signals, the 16/18 pair shows almost 9 ppm difference in chemical shift and resonance 18 is much broader, indicating a more drastic change in spin density on the proton. In combination with the observation that there are no other hydrogen bond acceptors in the proximity, this suggests that resonance 18 represents the His234 Hδ1 in a state in which the hydrogen bond to Asp259 is broken. In such a state the proton would be prone to exchange with bulk water protons but the TNC is very buried, preventing rapid exchange. Similar situations as for His102 are observed for other histidine ligands in the TNC (Table S3.4). in the crystal structure of SLAC from *S. griseoflavus*, (PDB entry 6s0o resolution 1.8 Å) (26) Nδ1 of His237 can form a hydrogen bond with Asp114 Oδ1 or water O540, depending on rotation around $\chi 2$ (Figure S3.5). In the crystal structure of SLAC from *S. coelicolor* (PDB entry: 3cg8, resolution 2.68 Å) the equivalent Asp113 Oδ1 is moved away from the Nδ1 and therefore could not form a hydrogen bond (Figure S3.5a). Such exchange processes may well represent the resonances pair 3-5 and 9-11. Second-shell mutations around the respective histidine residues can help to confirm this hypothesis.

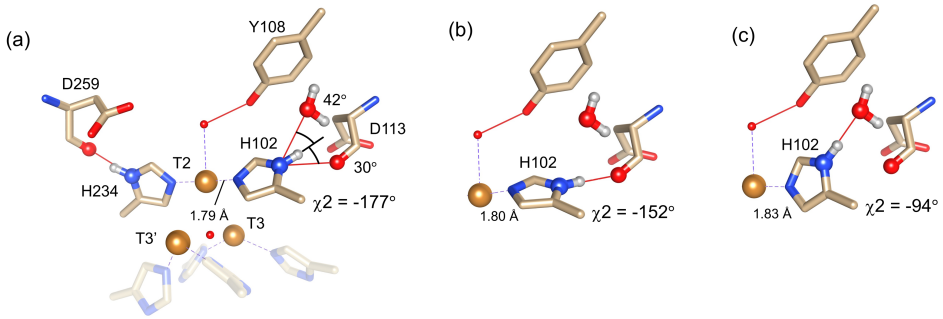


***Figure 3.4**. Alternative hydrogen bond acceptors for His102. (a) T2 site histidine ligands showing the hydrogen bonds for the Nδ1-Hδ1 group. Protons were modelled using the algorithm as implemented in UCSF Chimera (27). His104 and H236 from the T3' and T3 sites, respectively, are omitted for clarity. Hydrogen bonds are shown as red lines. The $\chi 2$ dihedral angle and distance between His102 Nε2 and the T2 copper are indicated. Also, the values for the angles [Asp113 CO – His102 Nδ1 – His102 Hδ1] and [water O628 – His102 Nδ1 – His102 Hδ1] are indicated. Ring rotation brings the Hδ1 in optimal position for hydrogen bond formation with either the Asp113 CO (b) or the water (c). The new $\chi 2$ dihedral angles and the corresponding His102 Nε2 — T2 copper distances are indicated.*

The temperature dependence of Hδ1 resonance is also affected by the Y108F mutation (Figure 3.5). While the resonances that show clear Curie behaviour in SLAC-T1D also do so in the Y108F mutant, resonances that show anti-Curie or non-Curie behaviour tend more to Curie like behaviour, e.g. resonances 3, 6, 7 and 8. The overall

increase in the Curie-like behaviour for the Y108F mutant compared to that of SLAC-T1D, can be due to the decrease in the *J* coupling between copper ions due to a change in the geometry of the TNC (28) caused by the loss of the hydrogen bond between the Tyr108 the water/hydroxide. Slight chemical shift changes are also present for the ^{1}H resonances between 10 and 20 ppm in the spectrum of SLAC-T1D/Y108F relative to that of SLAC-T1D (Figure S3.4). The ^{1}H-^{1}H EXSY/NOESY spectrum shows six cross-peaks (a to f), caused by 12 diagonal signals (Figure S3.4). Among these, a1, b1, c1, c2, d1 and e1 are downfield shifted for the mutant, whereas a2, b2, d2 and e2 are upfield shifted (Figure S3.4b).

In summary, the Y108F mutation leads to the following tentative assignment of the resonances: 13 and 12 to His102 and 16 to His234 of the T2 site, with 13 and 12 being in chemical exchange.

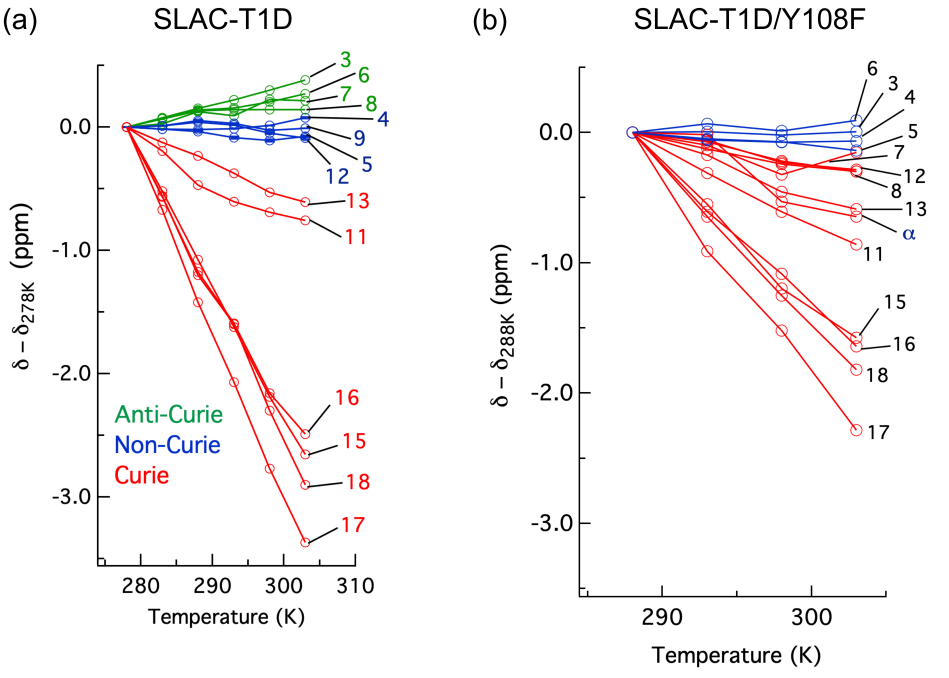


Figure 3.5. *Change in ^{1}H chemical shifts for (a) SLAC-T1D with temperature relative to 278 K and (b) SLAC-T1D/Y108F with temperature relative to 288 K. Anti-Curie, non-Curie and Curie behaviour are shown in green, blue and red, respectively.*

3.3 Conclusion

The SLAC-T1D comprises resonances from the NI and RO states, in which the RO state is the minor state.(13) Using differently labelled samples and a paramagnetically tailored ^{15}N–^{1}H HMQC experiment, all NI resonances of the Nδ1-Hδ1 groups of the eight coordinating histidine residues in the TNC were accounted for (Figure 3.1). The HMQC spectra also included the resonances that are in chemical exchange, consistent with the histidine ring motions being responsible for this phenomenon.(17) NOE cross-peaks for the RO state revealed resonances of Hβ protons of the coordinating histidine residues of the T3 site (Figure 3.2). The second shell mutation of Y108F of SLAC-T1D aided in the tentative assignment of the resonances 13 and 12 to His102 and 16 and 18 to His234 of the T2 site (Figures 3.3 and 3.4). This report shows the first sequential assignment of the paramagnetically shifted resonance to a coordinating histidine. More studies using second shell residue mutagenesis can help to provide a full sequence specific assignment, which is a prelude to a better understanding of the motions important for the catalytic mechanism

.

3.4 Supporting Information

Protein expression and purification

SLAC-T1D and SLAC-T1D/Y108F were expressed and purified as described previously. (17, 29) For ^{15}N histidine specific perdeuterated labelled sample, 50 mg/L of $^{15}N_3$-L-histidine hydrochloride monohydrate (Sigma Aldrich, USA) was added to the M9 medium consisting of ammonium chloride and D-glucose-1,2,3,4,5,6,6-d7 as nitrogen and carbon sources respectively. A volume of 200 µL of the M9 preculture was transferred to 25 mL of M9 medium prepared in 99.99% D_2O for an overnight preculture, which was used to inoculate 500 mL D_2O-M9 minimal medium. Gene expression and protein harvesting was done as for the uniform ^{15}N labelled sample. Purity was checked by SDS PAGE using a precast Bis-Tris gel (ThermoFischer scientific), as shown in Figure S3.1a. A band ~ 74 kDa is observed. Under native condition from size exclusion chromatography with multi-angle light scattering (SEC-MALS) the molecular weight of the proteins was ~ 105 kDa, in accord with the expected trimeric form.

NMR spectroscopy

Samples contained ~ 1 mM of protein in 10 mM sodium phosphate buffer pH 7.3 with 10% D_2O. Experiments were done on a Bruker AV-III HD 600 MHz NMR spectrometer equipped with a TXI cryoprobe. 1D ^1H WEFT, Inversion recovery experiments to measure the spin-lattice relaxation rate and 2D ^1H-^1H EXSY/NOESY (30) experiments were recorded as described previously (Chapter 2). (17) The mixing time dependent integral volume profiles were fitted using equations S2.1 to S2.4 (17, 31) with IGOR Pro 6.3.7 to obtain the exchange rates. The fitting was done by constraining the K_{eq} (Table S3.1) to the value of the ratio of the diagonal integral volume at mixing time of 0 ms. The spin-lattice relaxation rates used in the fitting were obtained from inversion recovery experiments.

2D ^{15}N–^1H HMQC experiments were recorded using the pulse sequence shown in Figure 1.5c and S3.2. The transfer delay d2 was optimized to 0.5 ms to enhance the paramagnetically shifted signals > 20 ppm. 48 t1 increment points were acquired with 30720 number of scans corresponding to the total acquisition time of 54 h for each experiment.

Supporting figures and tables

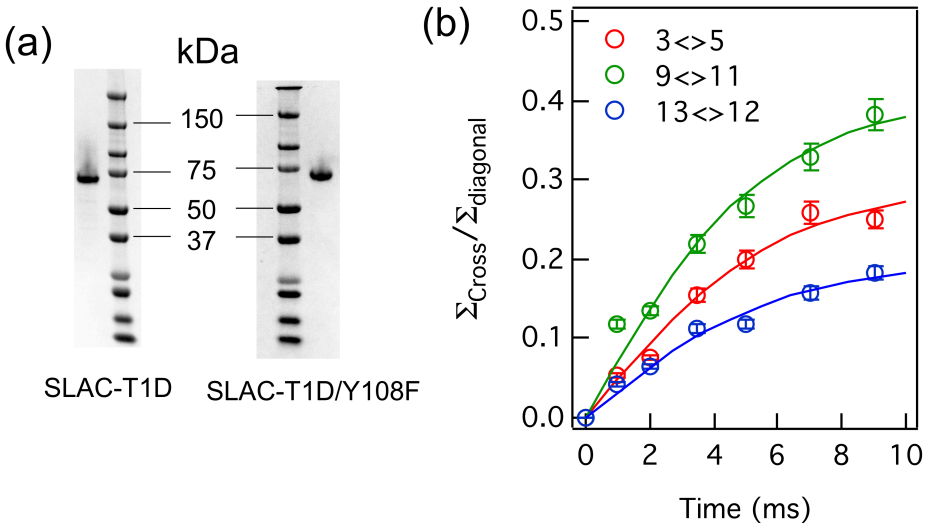


Figure S3.1*: (a) Image of a Bis-Tris precast SDS PAGE gel (ThermoFischer scientific) of purified SLAC-T1D and SLAC-T1D/Y108F; (b) Fits of the intensity profile of normalized cross peak integrals from the resonance pairs of 3-5, 9-11 and 13-12 from 2D ^{1}H-^{1}H EXSY of SLAC-T1D/Y108F to determine the exchange rates (17, 31). The error bars represent the standard error of the mean derived from the duplicate experiments.*

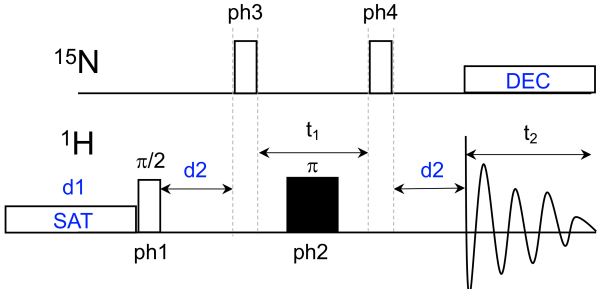


Figure S3.2. *^{15}N–^{1}H HMQC pulse sequence used in this study. Open rectangles are for 90° pulse and filled ones are for 180° pulse. The interscan delay d1 is 100 ms and SAT is the continuous wave water saturation pulse with phase of x. DEC is GARP composite pulse decoupling during the t_2 evolution. The evolution period d2 was set to 0.5 ms, corresponding to the FWHM of the paramagnetically shifted ^{1}H resonances (~ 0.8 ppm) (15, 18). The phase cycling is ph1 = x, ph2 = x, ph3 = x -x, ph4 = x x -x -x and for the receiver it was x -x x -x.*

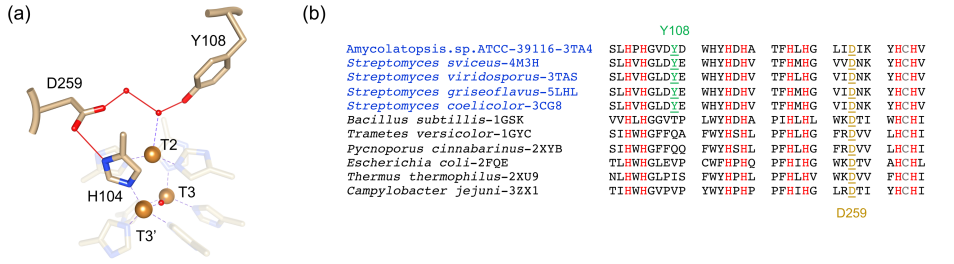


Figure S3.3. *The second coordination shell residue Tyr108. (a) Crystal structure of SLAC (PDB entry 3cg8, resolution 2.63 Å) (32), showing the hydrogen bonding network between Tyr108 and His104 via Asp259 (red lines). The hydrogen bonds were determined by the default parameter of UCSF Chimera program (27) with relaxed hydrogen bond constraints of 0.4 Å and 20.0° (Mills and Dean, 1996); (b) Sequence alignment of the two-domain (blue) and three-domain laccases (black) for which crystal structures are available (PDB code indicated). The copper coordinating residues are shown in red. Tyr108 and Asp259 (numbering from PDB 3cg8) are shown in green and gold, respectively and are underlined. The type 1 copper site ligand, cysteine, is marked in grey.*

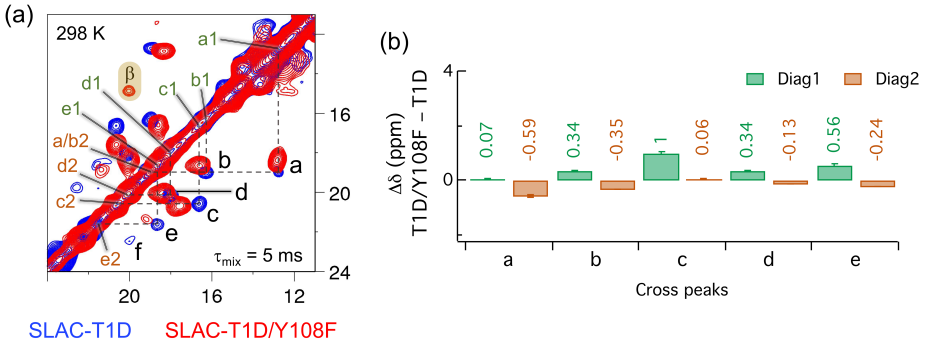


Figure S3.4. *Comparison of the RO spectral regions for SLAC-T1D and SLAC-T1D/Y108F. (a) Overlaid ^{1}H-^{1}H EXSY/NOESY spectra at 298 K with mixing time of 5 ms of SLAC-T1D (blue) and SLAC-T1D/Y108F (red) for the region between 11 and 22 ppm. Cross-peaks and diagonal peaks for SLAC-T1D are marked. Diagonal peaks are marked as a1, a2, b1, b2 etc. The new cross peak β in SLAC-T1D/Y108F is highlighted; (b) Chemical shift changes between SLAC-T1D and SLAC-T1D/Y108F. Positive values mean the diagonal peak in SLAC-T1D/Y108F is downfield shifted, while for the negative value it is upfield shifted. Diagonal peak 1 (Diag1: a1, b1, c1, d2 and e1) are shown in green while diagonal peaks 2 (Diag2: a2, b2, c2, d2, and e2) are shown in light brown. Resonance f and b are not shown since they are unique to SLAC-T1D and SLAC-T1D/Y108F respectively. More experiments are needed to identify these resonances.*

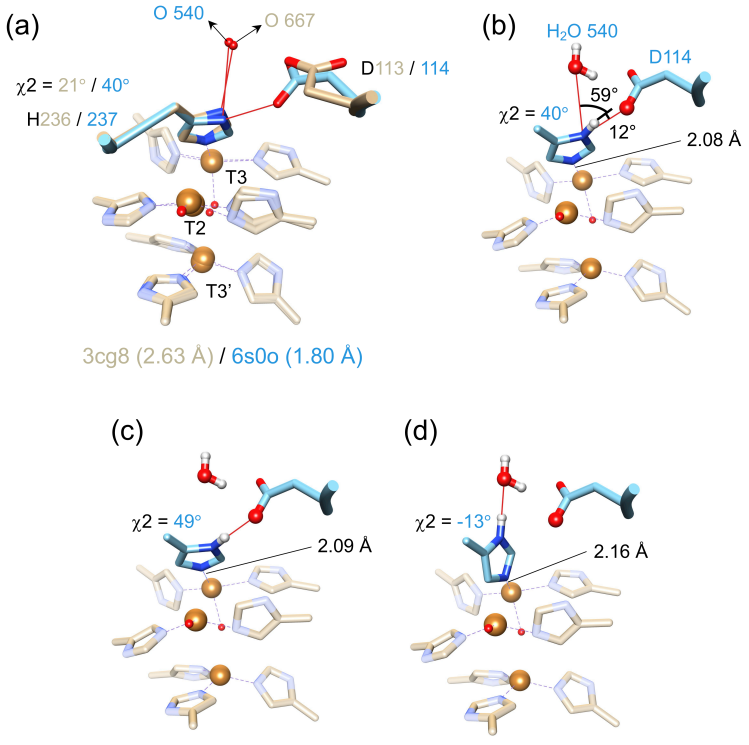


Figure S3.5. *Two H-bond acceptors for His236. (a) Overlaid TNC from crystal structure 3cg8 in gold and 6s0o in blue highlighting the hydrogen bond of the Nδ1 from the T3 histidine ligand His236/237 (26, 32). The χ2 dihedral angle for histidine 236/237 is shown for both crystal structures. Hydrogen bonds are shown as red lines; (b) Protons are modelled for the crystal structure 6s0o using the algorithm as implemented in UCSF Chimera (26, 27). The values of the angles between [Asp114 Oδ1 – His237 Nδ1 – His237 Hδ1] and [water O540 – His237 Nδ1 – His237 Hδ1] are indicated along with the distance between His237 Nε2 - T3 copper (with arrows); (c, d) The ring rotation that brings the Hδ1 to the optimal position for a hydrogen bond with Asp114 Oδ1 (c) and the water (d) are shown. The new χ2 dihedral angle and the corresponding His237 Nε2 - T3 copper distances are indicated.*

Table S3.1*. Exchange and spin lattice relaxation rates at 298 K for SLAC-T1D/Y108F. In brackets the values for SLAC-T1D are shown for comparison (17).* R_{1A} *and* R_{1B} *are the spin-lattice relaxation rates for state A and B respectively. Errors in the values are ~ 5% from the duplicate experiments.*

	3 – 5	9 – 11	13 – 12
k_A (s^{-1})	37 (33)	51 (29)	26 (29)
k_B (s^{-1})	60 (62)	91 (91)	39 (34)
k_{ex} (s^{-1})	97 (95)	142 (120)	65 (63)
K_{eq} (k_A/k_B)	0.62 (0.53)	0.56 (0.32)	0.67 (0.85)
R_{1A} (s^{-1})	225 (225)	240 (240)	170 (170)
R_{1B} (s^{-1})	518 (457)	524 (464)	483 (492)

Table S3.2. *^{1}H and ^{15}N chemical shift in ppm of the paramagnetically shifted resonances (> 21 ppm in 1D ^{1}H WEFT spectrum) at 298 K. Resonance showing no change between SLAC-T1D/Y108F and SLAC-T1D are highlighted. Resonance pairs undergoing chemical exchange are color coded as red for 3-5, green for 9-11 and blue for 13-12. ^{15}N chemical shift of resonance 7, 8, 17 and 18 are not observed from the ^{15}N-^{1}H HMQC spectra. Resonance 7 and 8 were reported to be carbon attached protons (17) while the ^{1}H resonance of 17 and 18 are broad (~ 1.1 ppm), which can affect the evolution period d2 in the ^{15}N-^{1}H HMQC (Figure S3.2). Since the d2 was set to 0.5 ms, corresponding to the ^{1}H line with of 0.8 ppm (Figure 2.1) at 600 MHz, resonance 17 and 18 might not be observable due to their large line broadening.*

Resonance	SLAC-T1D		SLAC-T1D/Y108F	
	^{1}H	^{15}N	^{1}H	^{15}N
3	22.00	291.65	22.24	294.24
4	23.40	245.21	24.53	251.16
5	24.75	330.35	25.07	333.41
6	26.46	461.91	25.95	459.73
7	29.26	-	29.26	-
8	31.65	-	31.65	-
9	34.88	450.30	35.43	456.79
11	36.95	477.39	37.68	485.19
12	39.24	535.44	39.20	539.05
13	41.82	581.87	42.04	565.49
15	43.09	569.04	43.13	570.38
16	44.11	574.13	43.67	559.61
17	49.17	-	49.17	-
18	52.52	-	52.52	-

***Table S3.3**. ^{1}H and ^{15}N chemical shift in ppm at 298 K for the resonance between 12 and 21 ppm of the RO state.*

Resonance	SLAC-T1D	
	^{1}H	^{15}N
a1	12.82	179
a2	19.01	266
b1	16.29	-
b2	19.06	270
c1	16.65	248
c2	20.59	277
d1	18.01	-
d2	20.02	275
e1	18.64	-
e2	21.64	-
x1	13.58	185
x2	14.68	213
y	15.43	232
w	13.29	190
z	19.90	265

***Table S3.4**. Potential hydrogen bond acceptors for T3 His Nδ1 atoms as defined by (33). Data based on chains E and F from PDB entry 6s0O (resolution 1.80Å) (26).*

Histidine	Potential hydrogen bond acceptors
His 105.E	Asp 260.F Oδ1 and H_2O 546.E O
His 290.F	Gln 292.F Oε1 and H_2O 540.F O
His 159.E	Glu 164.E CO and H_2O 540.E O
His 237.F	Asp 114.E Oδ1 and H_2O 501.E O

Table S3.5*. The estimated hyperfine constant A from the fit in of the chemical shift temperature dependence in Figure 3.2b of the main text using equation 1.5.*

Resonance	Hyperfine coupling constant *A* (MHz)
a1	0.7 +/- 0.2
b1	2.7 +/- 0.3
c1	1.5 +/- 0.1
d1	3.0 +/- 0.5
a2	2.0 +/- 0.2
b2	2.0 +/- 0.2
c2	2.3 +/- 0.4
d2	2.2 +/- 0.3

3.5 References

1. Gupta, A., I. Nederlof, S. Sottini, A.W.J.W. Tepper, E.J.J. Groenen, E.A.J. Thomassen, and G.W. Canters. 2012. Involvement of Tyr108 in the Enzyme Mechanism of the Small Laccase from *Streptomyces coelicolor*. *Journal of the American Chemical Society*. 134:18213–18216.
2. Heppner, D.E., C.H. Kjaergaard, and E.I. Solomon. 2014. Mechanism of the Reduction of the Native Intermediate in the Multicopper Oxidases: Insights into Rapid Intramolecular Electron Transfer in Turnover. *J. Am. Chem. Soc.* 136:17788–17801.
3. Quintanar, L., J. Yoon, C.P. Aznar, A.E. Palmer, K.K. Andersson, R.D. Britt, and E.I. Solomon. 2005. Spectroscopic and Electronic Structure Studies of the Trinuclear Cu Cluster Active Site of the Multicopper Oxidase Laccase: Nature of Its Coordination Unsaturation. *J. Am. Chem. Soc.* 127:13832–13845.
4. Tepper, A.W.J.W., S. Milikisyants, S. Sottini, E. Vijgenboom, E.J.J. Groenen, and G.W. Canters. 2009. Identification of a Radical Intermediate in the Enzymatic Reduction of Oxygen by a Small Laccase. *J. Am. Chem. Soc.* 131:11680–11682.
5. Yoon, J., and E.I. Solomon. 2007. Electronic Structure of the Peroxy Intermediate and Its Correlation to the Native Intermediate in the Multicopper Oxidases: Insights into the Reductive Cleavage of the O−O Bond. *J. Am. Chem. Soc.* 129:13127–13136.
6. Kielb, P., H.B. Gray, and J.R. Winkler. 2020. Does Tyrosine Protect *S. Coelicolor* Laccase from Oxidative Degradation? DOI: 10.26434/chemrxiv.12671612.v1
7. Tian, S., S.M. Jones, and E.I. Solomon. 2020. Role of a Tyrosine Radical in Human Ceruloplasmin Catalysis. *ACS Cent. Sci.* DOI: 10.1021/acscentsci.0c00953
8. Hammes-Schiffer, S. 2006. Hydrogen Tunneling and Protein Motion in Enzyme Reactions. *Acc. Chem. Res.* 39:93–100.
9. Hammes-Schiffer, S., and S.J. Benkovic. 2006. Relating Protein Motion to Catalysis. *Annual Review of Biochemistry*. 75:519–541.
10. Henzler-Wildman, K.A., V. Thai, M. Lei, M. Ott, M. Wolf-Watz, T. Fenn, E. Pozharski, M.A. Wilson, G.A. Petsko, M. Karplus, C.G. Hübner, and D. Kern. 2007. Intrinsic motions along an enzymatic reaction trajectory. *Nature*. 450:838–844.
11. Poulos, T.L. 2003. Cytochrome P450 flexibility. *Proceedings of the National Academy of Sciences*. 100:13121–13122.
12. Dasgupta, R., K.B.S.S. Gupta, F. Nami, H.J.M. de Groot, G.W. Canters, E.J.J. Groenen, and M. Ubbink. 2020. Chemical Exchange at the Trinuclear Copper Center of Small Laccase from *Streptomyces coelicolor*. *Biophysical Journal*. 119:9–14.

13. Machczynski, M.C., and J.T. Babicz. 2016. Correlating the structures and activities of the resting oxidized and native intermediate states of a small laccase by paramagnetic NMR. *Journal of Inorganic Biochemistry*. 159:62–69.
14. Zaballa, M.-E., L. Ziegler, D.J. Kosman, and A.J. Vila. 2010. NMR Study of the Exchange Coupling in the Trinuclear Cluster of the Multicopper Oxidase Fet3p. *J. Am. Chem. Soc.* 132:11191–11196.
15. Ciofi-Baffoni, S., A. Gallo, R. Muzzioli, and M. Piccioli. 2014. The IR-^{15}N-HSQC-AP experiment: a new tool for NMR spectroscopy of paramagnetic molecules. *Journal of Biomolecular NMR*. 58:123–128.
16. Gelis, I., N. Katsaros, C. Luchinat, M. Piccioli, and L. Poggi. 2003. A simple protocol to study blue copper proteins by NMR. *European Journal of Biochemistry*. 270:600–609.
17. Dasgupta, R., K.B.S.S. Gupta, F. Nami, H.J.M. de Groot, G.W. Canters, E.J.J. Groenen, and M. Ubbink. 2020. Chemical Exchange at the Trinuclear Copper Center of Small Laccase from *Streptomyces coelicolor*. *Biophysical Journal*. 119:9–14.
18. Bertini, I., C. Luchinat, G. Parigi, and E. Ravera. 2017. NMR of paramagnetic molecules: applications to metallobiomolecules and models. Second edition. Amsterdam: Elsevier.
19. Banci, L., I. Bertini, and C. Luchinat. 1990. The ^{1}H NMR parameters of magnetically coupled dimers—The Fe2S2 proteins as an example. In: Bioinorganic Chemistry. Berlin, Heidelberg: Springer. pp. 113–136.
20. Bubacco, L., E. Vijgenboom, C. Gobin, A.W.J.W. Tepper, J. Salgado, and G.W. Canters. 2000. Kinetic and paramagnetic NMR investigations of the inhibition of *Streptomyces antibioticus* tyrosinase. *Journal of Molecular Catalysis B: Enzymatic*. 8:27–35.
21. Tepper, A.W.J.W., L. Bubacco, and G.W. Canters. 2006. Paramagnetic Properties of the Halide-Bound Derivatives of Oxidised Tyrosinase Investigated by ^{1}H NMR Spectroscopy. *Chem. Eur. J.* 12:7668–7675.
22. Battistuzzi, G., G. Di Rocco, A. Leonardi, and M. Sola. 2003. ^{1}H NMR of native and azide-inhibited laccase from *Rhus vernicifera*. *Journal of Inorganic Biochemistry*. 96:503–506.
23. Quintanar, L., C. Stoj, T.-P. Wang, D.J. Kosman, and E.I. Solomon. 2005. Role of Aspartate 94 in the Decay of the Peroxide Intermediate in the Multicopper Oxidase Fet3p. *Biochemistry*. 44:6081–6091.
24. Bertini, Ivano., Paola. Turano, and A.J. Vila. 1993. Nuclear magnetic resonance of paramagnetic metalloproteins. *Chem. Rev.* 93:2833–2932.
25. Patt, S.L., and B.D. Sykes. 1972. Water Eliminated Fourier Transform NMR Spectroscopy. *J. Chem. Phys.* 56:3182–3184.
26. Gabdulkhakov, A., I. Kolyadenko, O. Kostareva, A. Mikhaylina, P. Oliveira, P. Tamagnini, A. Lisov, and S. Tishchenko. 2019. Investigations of Accessibility of T2/T3 Copper Center of Two-Domain Laccase from *Streptomyces griseoflavus* Ac-993. *International Journal of Molecular Sciences*. 20:3184.
27. Pettersen, E.F., T.D. Goddard, C.C. Huang, G.S. Couch, D.M. Greenblatt, E.C. Meng, and T.E. Ferrin. 2004. UCSF Chimera—A visualization system for exploratory research and analysis. *Journal of Computational Chemistry*. 25:1605–1612.
28. Solomon, E.I., A.J. Augustine, and J. Yoon. 2008. O_2 Reduction to H_2O by the multicopper oxidases. *Dalton Trans.* 3921–3932.
29. Machczynski, M.C., E. Vijgenboom, B. Samyn, and G.W. Canters. 2004. Characterization of SLAC: A small laccase from *Streptomyces coelicolor* with unprecedented activity. *Protein Science*. 13:2388–2397.
30. Jeener, J., B.H. Meier, P. Bachmann, and R.R. Ernst. 1979. Investigation of exchange processes by two-dimensional NMR spectroscopy. *J. Chem. Phys.* 71:4546–4553.
31. Farrow, N.A., O. Zhang, J.D. Forman-Kay, and L.E. Kay. 1994. A heteronuclear correlation experiment for simultaneous determination of ^{15}N longitudinal decay and chemical exchange rates of systems in slow equilibrium. *J Biomol NMR*. 4:727–734.
32. Skálová, T., J. Dohnálek, L.H. Østergaard, P.R. Østergaard, P. Kolenko, J. Dušková, A. Štěpánková, and J. Hašek. 2009. The Structure of the Small Laccase from *Streptomyces coelicolor* Reveals a Link between Laccases and Nitrite Reductases. *Journal of Molecular Biology*. 385:1165–1178.
33. Mills, J.E.J., and P.M. Dean. 1996. Three-dimensional hydrogen-bond geometry and probability information from a crystal survey. *J Computer-Aided Mol Des*. 10:607–622.